JOURNAL OF SOLID STATE CHEMISTRY 105, 49–69 (1993)

The Structure and Spectroscopic Properties of $Al_{2-x}Cr_x(WO_4)_3$ Crystals in Orthorhombic and Monoclinic Phases

J. HANUZA, M. MACZKA, K. HERMANOWICZ,
M. ANDRUSZKIEWICZ, A. PIETRASZKO, W. STREK, AND P. DEREŃ

Institute for Low Temperatures and Structure Research, Polish Academy of Sciences, Wrocław, Poland

Received July 20, 1992; in revised form October 29, 1992; accepted November 2, 1992

The structure and spectroscopic properties of Cr^{3+} doped $Al_2(WO_4)_3$ crystals in orthorhombic and monoclinic phases are studied and compared. On the basis of absorption, emission, IR, Raman scattering, and lifetime measurements the different Cr^{3+} centers are analyzed and characterized. The results obtained are related to those of other authors.

Introduction

Divalent ABO_4 tungstates and molybdates, as well as trivalent $A_2(BO_4)_3$ compounds, have been examined as suitable host lattices for transition metal ions. The spectroscopic properties of $ZnWO_4$, $CdWO_4$, $Al_2(WO_4)_3$, and $Sc_2(WO_4)_3$ crystals doped with Cr^{3+} were studied by Nosenko and Futorski (*1*) and Peterman and co-workers (*2–4*). Laser action has been observed in $Zn_{1-x}Cr_xWO_4$ and $Al_{2-x}Cr_x(WO_4)_3$ materials (*3, 4*). For the last compound a phase transition at about 210 K was reported, but without any details (*4*). In the present work we employ several spectroscopic techniques to study this transition. We report X-ray, IR, and polarized Raman data as well as absorption and emission spectra as functions of Cr^{3+} concentration and temperature. The concentration quenching of luminescence for $Al_{2-x}Cr_x(WO_4)_3$ crystal doped with $x = 0.004$, 0.01, 0.02, and 0.04 chromium content was investigated. These results are important for understanding the mechanisms of cooperative interactions, which are responsible for the dynamics of luminescence, energy transfer, and diffusion of energy in crystals. The structure and properties of both phases, orthorhombic and monoclinic, are analyzed and a transition mechanism is proposed.

Experimental Procedures

The synthesis of crystals was carried out using the flux method described in (*4, 5*). We grew $3 \times 3 \times 2$ mm^3 single crystals from platinum crucibles. The $Al_2(WO_4)_3$ (ALWO) crystal is colorless and optically transparent. Doping with chromium(III) ions gives it a pale yellow color. The Cr^{3+} concentration in the host was determined by means of a calibration curve, by measuring the optical density of the 21,300 cm^{-1} peak as a function of the active ion content.

The crystal phases obtained were identified by single crystal X-ray diffraction with Mo$K\alpha$ 0.71073 Å radiation using a four circle KUMA diffractometer KM 4. The redetermination of the $Al_2(WO_4)_3$ structure at RT was performed for the 6035 measured reflections (3230 unique ones, 1965 with $I > 3\delta$) with final discrepancy factors $R = 0.0319$ and $R_W = 0.0316$. The structure of the monoclinic phase was determined at 160 K using

0022-4596/93 $5.00

Cu$K\alpha$ radiation. The X-ray measurements were performed in the temperature range 300 to 120 K. The low temperature Oxford Cryosystem attachment was used.

IR spectra were taken in a Bruker IFS 88 FT-IR spectrometer and Raman spectra in an Yvon Jobin U1000 spectrophotometer using the 5140-Å line from an argon laser (Spectra Physics 2016).

The electron absorption spectra were recorded by a Cary 2300 Varian UV–VIS–NIR Spectrophotometer.

The emission spectra measurement and the lifetime experiment were done in a TH1000 Jobin Yvon Spectrometer. Krypton ILK120 and argon IKA120 lasers were used as excitation sources. For decay time measurements an Sr400-Stanford Research gated photon counter system was used, with excimer laser (LPX100-Lambda Physik) excitation.

The Structure of $Al_2(WO_4)_3$ and Its Phase Transition

The $Al_2(WO_4)_3$ in the 210–300 K temperature range is orthorhombic with space group $Pbcn = D_{2h}^{14}$ and with four formula units per unit cell. The lattice parameters at 293 K are $a = 12.571$; $b = 9.046$, and $c = 9.129$ Å. Atomic coordinates and selected interatomic distances are presented in Tables I and II. The parameters of the crystal structure at RT agree with the results reported by Boer (*6*) and slightly differ from those found by Craig and Stephenson (*7*). Figure 1 presents the crystal structure of the orthorhombic phase along c axis and in the ac projection.

In the host discussed the Cr^{3+} ions substitute the 8*d* position occupied by aluminum(III) ions. The activator is surrounded by oxygen ions in a slightly distorted octahedral arrangement. The site symmetry of this polyhedron is C_1, but the local symmetry can be regarded as close to the tetragonal C_{4v} symmetry because the Al–O(3) distance significantly differs from the other ones.

The position and intensity of the selected reflections as functions of the temperature were examined by the single crystal X-ray diffraction method. The plot of lattice parameters vs temperature reveals a phase transition of the first order at 210 K (±1 K)

TABLE I

REDETERMINATION OF THE ORTHORHOMBIC $Al_2(WO_4)_3$ STRUCTURE ($Pbcn = D_{2h}^{14}$, $Z = 4$)

	Positional and anisotropic thermal parameters of the atoms U_{ij}(Å^2)								
W.p. atom	*X/A*	*Y/B*	*Z/C*	*U*11	*U*22	*U*33	*U*23	*U*13	*U*12
4c2W1	0.00000	0.47452	0.25000	0.00748	0.00441	0.00382	0.00000	0.00025	0.00000
	0.00000	0.00006	0.00000	0.00017	0.00016	0.00016	0.00000	0.00014	0.00000
8*d*1W2	0.35549	0.39579	0.11795	0.00324	0.00682	0.00561	0.00163	−0.00051	−0.00030
	0.00003	0.00004	0.00004	0.00012	0.00013	0.00013	0.00010	0.00010	0.00010
8*d*1AL	0.38022	0.24947	0.46575	0.00501	0.00448	0.00623	−0.00085	−0.00001	0.00103
	0.00024	0.00035	0.00034	0.00092	0.00104	0.00105	0.00084	0.00081	0.00084
8*d*1O1	0.14260	0.09008	0.09305	0.02221	0.01236	0.01035	0.00957	−0.00071	0.00472
	0.00079	0.00097	0.00094	0.00333	0.00292	0.00264	0.00231	0.00248	0.00270
8*d*1O2	0.06723	0.36638	0.12258	0.01819	0.01689	0.01589	−0.01053	0.00134	0.00630
	0.00081	0.00107	0.00102	0.00314	0.00308	0.00296	0.00264	0.00274	0.00285
8*d*1O3	0.25500	0.31493	0.00640	0.01342	0.02363	0.01539	−0.00307	−0.00616	−0.00091
	0.00074	0.00119	0.00103	0.00265	0.00347	0.00290	0.00286	0.00263	0.00277
8*d*1O4	0.40580	0.08845	0.33829	0.01279	0.01119	0.02141	−0.00936	0.00558	0.00515
	0.00069	0.00095	0.00108	0.00274	0.00286	0.00326	0.00254	0.00258	0.00233
8*d*1O5	0.47860	0.31672	0.07021	0.00897	0.01705	0.01610	0.00228	0.00140	0.00324
	0.00064	0.00108	0.00103	0.00240	0.00306	0.00289	0.00262	0.00231	0.00244
8*d*1O6	0.33162	0.36316	0.30595	0.00961	0.02478	0.00675	0.01075	0.00199	0.00830
	0.00067	0.00110	0.00087	0.00247	0.00346	0.00241	0.00243	0.00209	0.00255

Discrepancy factors

$R = 0.0323$ $R_w = 0.0387$ $R_g = wR = 0.0612$

Note. Cell 12.571, 9.046, 9.129, 90.00, 90.00, 90.00. Total of G035 reflections, 1965 unique reflections; Mo radiation, 0.71009 Å.

TABLE II

SOME STRUCTURAL DATA FOR $Al_2(WO_4)_3$ IN ORTHORHOMBIC PHASE

W1–O2	1.739(0.010)	O1–O2	2.687(0.013)	O4–O6	2.671(0.013)
W1–O2 B	1.739(0.010)	O1–O3	2.600(0.014)	O4–O2 A	2.649(0.014)
W1–O4 B	1.765(0.009)	O1–O5 C	2.680(0.013)	O4–O3 A	2.684(0.013)
W1–O4 D	1.765(0.009)	O1–O6 A	2.675(0.012)	O4–O5 B	2.660(0.013)
W2–O3	1.780(0.010)	O2–O1	2.687(0.013)	O5–O1 B	2.680(0.013)
W2–O5	1.760(0.008)	O2–O3	2.629(0.014)	O5–O2 C	2.661(0.013)
W2–O6	1.767(0.008)	O2–O4 A	2.649(0.014)	O5–O4 C	2.660(0.013)
W2–O1 C	1.772(0.009)	O2–O5 C	2.661(0.013)	O5–O6 B	2.673(0.012)
Al–O4	1.892(0.010)	O3–O1	2.600(0.014)	O6–O4	2.671(0.013)
Al–O6	1.887(0.009)	O3–O2	2.629(0.014)	O6–O1 A	2.675(0.012)
Al–O1 A	1.881(0.009)	O3–O4 A	2.684(0.013)	O6–O3 A	2.670(0.013)
Al–O2 A	1.893(0.010)	O3–O6 A	2.670(0.013)	O6–O5 B	2.673(0.012)
Al–O3 A	1.835(0.010)				
Al–O5 B	1.905(0.009)				

Note. Bond lengths are in Å.

(Fig. 2). The transition from the orthorhombic to the monoclinic system occurs with a small deformation of the lattice parameters (about 0.05° at 40 K below the transition point). Below T_c the broadening and splitting of the X-ray reflections is observed, indicating that a twinned structure is formed in the crystal. The intensity data for low-temperature phase refer to 160 K where monoclinic space group $P2_1$ ($P2_1/n$) exists (a = 8.962 Å, b = 9.080 Å, c = 12.587 Å, and β = 90.06°). In Tables III and IV preliminary results of the atomic coordinates are shown for the $P2_1$ space group (discrepancy factor 8.96%). X-ray results determined for ALWO crystals suggest that at low temperature this phase can be ferroelastic.

IR and Polarized Raman Spectra

The high temperature orthorhombic phase of $Al_2(WO_4)_3$ contains 68 atoms in the

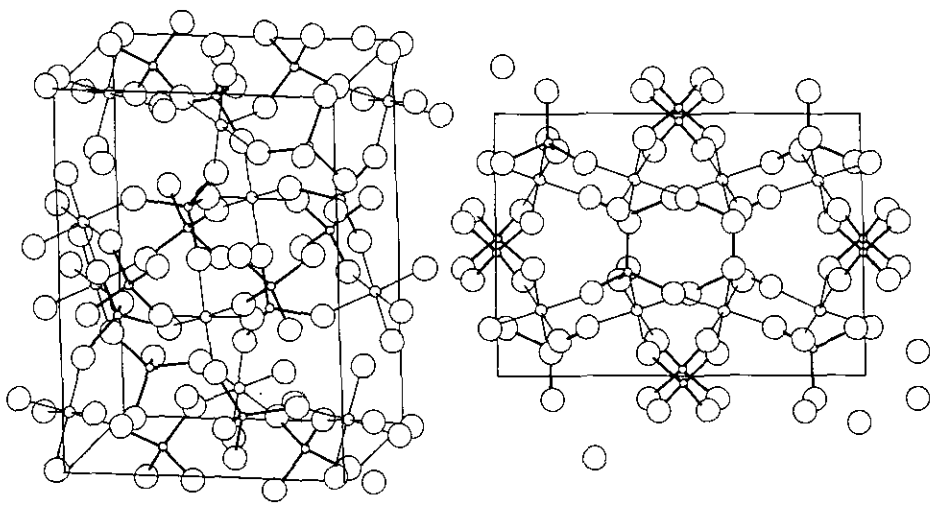

FIG. 1. The structure of the $Al_2(WO_4)_3$ unit cell.

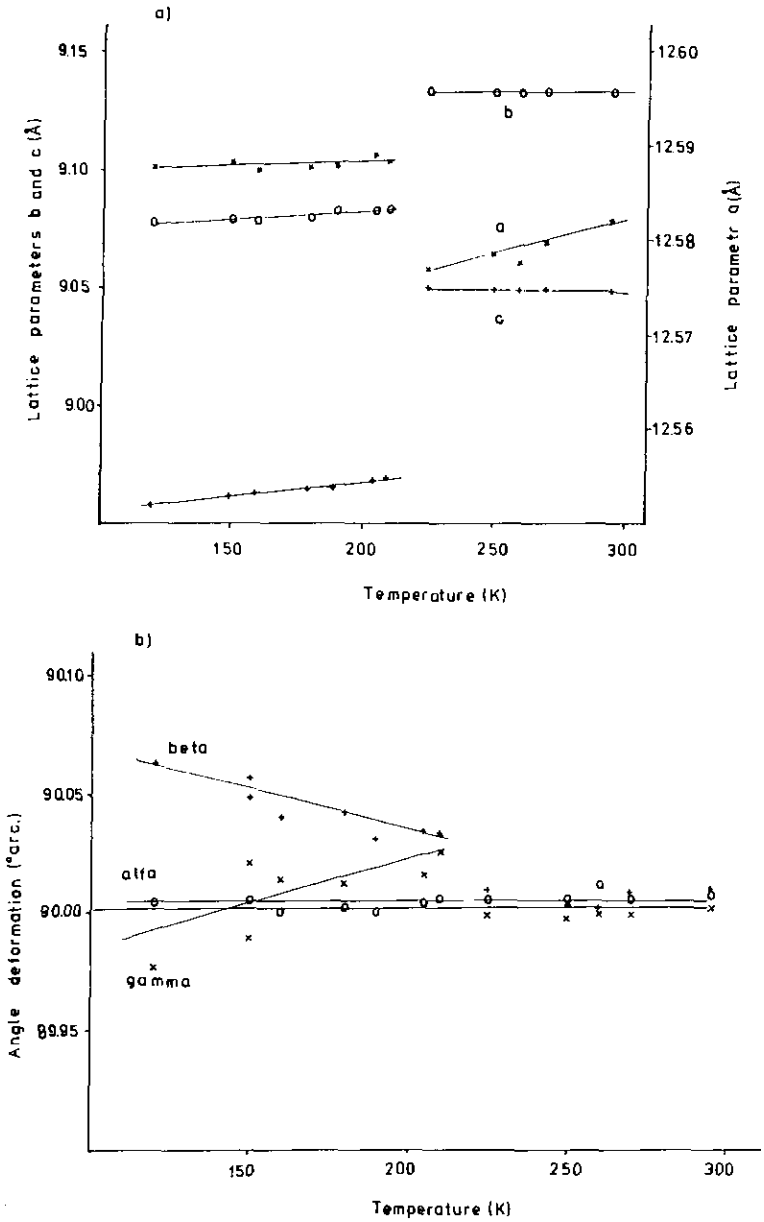

FIG. 2. Lattice parameters vs temperature for the $Al_2(WO_4)_3$ crystal.

unit cell. This leads to 204 vibrational $\mathbf{K} = 0$ degrees of freedom, which are described by the following representation:

$$\Gamma = 25A_g + 26B_{1g} + 25B_{2g} + 26B_{3g} + 25A_u + 26B_{1u} + 25B_{2u} + 26B_{3u}.$$

Its distribution among acoustic (T), translational (T'), librational (L), and internal i-modes is presented in Table V.

In order to obtain all modes of the unit cell one should record seven polarized spectra, four Raman and three IR ones. The Raman active A_g, B_{1g}, B_{2g}, and B_{3g} modes may be measured in (xx, yy, zz), xy, xz, and yz spec-

TABLE III

X-RAY DATA FOR $Al_2(WO_4)_3$ IN MONOCLINIC $P2(1)$ PHASE

Atom	Positional and thermal parameters of the atoms			
	X/A	*Y/B*	*Z/C*	*Ueq*[a]
W1	0.22199	0.25466	0.75191	0.00210
	0.00023	0.00122	0.00000	0.00055
W2	0.27510	0.75498	0.75098	0.00320
	0.00023	0.00122	0.00018	0.00055
W3	0.14086	0.12147	0.10413	0.00445
	0.00027	0.00122	0.00023	0.00059
W4	0.35427	0.88327	0.39244	0.00558
	0.00027	0.00123	0.00022	0.00060
W5	0.63813	0.11243	−0.10596	0.00269
	0.00025	0.00121	0.00020	0.00056
W6	−0.15216	0.87516	0.60471	0.00210
	0.00024	0.00121	0.00019	0.00054
Al1	−0.00208	0.47201	0.13695	0.00310
	0.00151	0.00196	0.00129	0.00254
Al2	0.50342	0.53480	0.37342	0.00161
	0.00161	0.00197	0.00136	0.00248
Al3	0.50599	0.47383	−0.12879	0.00310
	0.00153	0.00197	0.00131	0.00246
Al4	−0.01712	0.52912	0.64517	0.00985
	0.00204	0.00225	0.00157	0.00292
O11	0.12929	0.10985	0.81247	0.02210
	0.00287	0.00267	0.00229	0.00447
O12	0.09225	0.38267	0.70877	0.05374
	0.00378	0.00377	0.00374	0.00590
O13	0.32871	0.18565	0.64819	0.06298
	0.00422	0.00457	0.00274	0.00595
O14	0.33819	0.32993	0.84657	0.00534
	0.00309	0.00350	0.00220	0.00487
O21	0.16741	0.62844	0.68087	0.03363
	0.00379	0.00364	0.00308	0.00566
O22	0.37137	0.87327	0.66845	0.01127
	0.00304	0.00302	0.00225	0.00463
O23	0.40336	0.65109	0.82343	0.05149
	0.00374	0.00409	0.00329	0.00586
O24	0.15801	0.84583	0.84110	0.01010
	0.00269	0.00307	0.00201	0.00437
O31	0.12114	0.31416	0.09990	0.00910
	0.00317	0.00204	0.00251	0.00449
O32	0.33355	0.08656	0.10840	0.01210
	0.00176	0.00333	0.00247	0.00448
O33	0.08044	0.05948	0.22792	0.02110
	0.00294	0.00311	0.00158	0.00441
O34	0.06181	0.02886	−0.00098	0.01020
	0.00298	0.00305	0.00183	0.00440
O41	0.46447	0.91982	0.27980	0.01320
	0.00273	0.00326	0.00173	0.00430
O42	0.42171	0.70573	0.42143	0.02130
	0.00298	0.00226	0.00252	0.00439
O43	0.16729	0.89456	0.36570	0.01135
	0.00182	0.00328	0.00252	0.00445
O44	0.40710	1.00386	0.49238	0.01879
	0.00376	0.00349	0.00234	0.00533
	0.82970	0.09362	−0.12906	0.01601
O51	0.00184	0.00356	0.00268	0.00466
	0.57925	−0.00504	−0.00669	0.02010
O52	0.00305	0.00292	0.00193	0.00444
	0.55070	0.08756	−0.22909	0.02857
O53	0.00386	0.00432	0.00191	0.00546
	0.61522	0.29670	−0.07045	0.05283
O54	0.00460	0.00248	0.00372	0.00588
	−0.34238	0.92106	0.60008	0.03210
O61	0.00184	0.00331	0.00251	0.00438
	−0.05817	0.97706	0.51034	0.04424
O62	0.00401	0.00404	0.00275	0.00573
	−0.08133	0.93143	0.72934	0.01879
O63	0.00377	0.00386	0.00185	0.00522
	−0.11948	0.68422	0.60141	0.03210
O64	0.00306	0.00205	0.00250	0.00450

Discrepancy factors

$R = 0.0846$ $R_w = 0.1023$ $R_g = wR = 0.1329$

Note. Cell 8.962, 9.080, 12.587, 90.00, 90.06, 90.00. Total of 4334 reflections, 4152 unique reflections; Cu radiation, 1-54178 Å.

[a]Isotropic equivalent thermal parameter (Å^2).

tra, respectively, where $x \parallel a$, $y \parallel b$, $z \parallel c$. The B_{1u}, B_{2u}, and B_{3u} spectra should be recorded by applying the polarization parallel to the c, b, and a axes, respectively. The $x(yy)z$ A_g, $y(xy)x$ B_{1g}, $y(xz)x$ B_{2g}, and $y(zy)x$ B_{3g} Raman spectra and the $\mathbf{E} \parallel y$, $\mathbf{E} \parallel z$ IR spectra are presented in Figs. 3 and 4 and compared with the spectra obtained for powders. The spectrum $\mathbf{E} \parallel x$ could not be measured because of the small dimension of the crystal in this direction.

The isolated WO_4^{3-} ion has T_d symmetry with four fundamental vibrations at $\nu_1(A_1)$ 928, $\nu_2(E)$ 320, $\nu_3(F_2)$ 833, and $\nu_4(F_2)$ 405 cm^{-1} (*8, 9*). According to the X-ray data, WO_4^{2-} ions occupy two different positions of C_2 and C_1 site symmetry. The correlation diagram for the internal vibrations of the tungstate ions in $Al_2(WO_4)_3$ is given in Table VI. The energy level splitting and vibra-

TABLE IV

SOME STRUCTURAL DATA FOR MONOCLINIC $Al_2(WO_4)_3$ PHASE

W1–O12	1.731(0.037)	Al2–O42	1.820(0.029)
W1–O13	1.736(0.037)	Al2–O13 B	2.053(0.043)
W1–O14	1.723(0.028)	Al2–O22 A	1.921(0.032)
W1–O11	1.733(027)	Al2–O44 B	1.890(0.035)
W2–O21	1.740(0.036)	Al2–O53 B	1.940(0.031)
W2–O22	1.726(0.029)	Al2–O61 A	1.806(0.028)
W2–O23	1.744(0.037)	Al3–O43 A	2.021(0.036)
W2–O24	1.752(0.026)	Al3–O14 A	2.016(0.034)
		Al3–O23 A	1.949(0.041)
W3–O31	1.759(0.022)	Al3–O32 A	1.783(0.027)
W3–O32	1.757(0.017)	Al3–O41 B	1.981(0.028)
W3–O33	1.744(0.022)	Al3–O52 A	1.879(0.030)
W3–O34	1.720(0.026)		
		Al4–O12	1.835(0.042)
W4–O41	1.760(0.023)	Al4–O21	1.936(0.039)
W4–O42	1.760(0.024)	Al4–O64	1.776(0.030)
W4–O43	1.712(0.017)	Al4–O33 B	1.718(0.029)
W4–O44	1.733(0.031)	Al4–O43 B	1.823(0.030)
		Al4–O62 A	2.124(0.040)
W5–O51	1.750(0.018)	Al1–O31	1.869(0.028)
W5–O52	1.726(0.027)	Al1–O11 C	1.809(0.030)
W5–O53	1.751(0.027)	Al1–O24 B	1.828(0.030)
W5–O54	1.744(0.027)	Al1–O34 B	1.866(0.029)
		Al1–O51 B	1.902(0.028)
W6–O61	1.756(0.018)	Al1–O63 B	1.877(0.030)
W6–O62	1.726(0.036)		
W6–O63	1.767(0.026)		
W6–O64	1.750(0.022)		

Note. Bond lengths are in Å.

tional frequencies are also proposed. Complete vibrational data for the orthorhombic phase are listed in Table VII.

A similar analysis was performed for the low-temperature modification of $Al_2(WO_4)_3$. Table VIII gives the factor group analysis for the monoclinic phase. Figure 5 and Table IX present the experimental data for this structure.

Redistributions of the main spectral contours for both phases are nearly identical in the 100–1200 cm^{-1} region, although almost all bands occurring above 210 K are split below T_c into clear doublets or triplets (Fig. 5, Table IX). Such behavior agrees with the vibrational characteristics given in Tables V and VIII. The transition from the D_{2h}^{14} to C_2^2 structure destroys the center of symmetry and correlates the A_u, A_g, B_{2u}, and B_{2g} modes with the A ones and those of B_{1u}, B_{1g}, B_{3u}, B_{3g} symmetry with the B modes. For the low-temperature phase all modes became active both in IR and RS spectra. The temperature behavior of the spectral lines in the 100–1200 cm^{-1} region indicates that the structural changes that take place at the transition involve a change in relative orientational position of the WO_4 tetrahedra. This leads to twinning of the C_2^2 phase. A rotation of the tungstate units preserves the intranuclear forces inside them and therefore the lines of the 100–1200 cm^{-1} region do not show any change in frequency or line width across the transition at 210 K. Similar effects were described for phase transitions in $ABMX_4$ type compounds (*10*).

Electron Absorption Spectra

The absorption spectrum of $Al_{2-x}Cr_x(WO_4)_3$ in the orthorhombic phase was briefly discussed by Peterman and Mitzscherlich (*4*). Our results essentially agree with those published by these authors. In Fig. 6 the polarized absorption spectra of an $Al_{1.96}Cr_{0.04}(WO_4)_3$ orthorhombic crystal are shown. The results obtained are in accordance with tetragonal C_{4v} distortion of the CrO_6 polyhedron. The absorbances of all bands are very high due to the lifting of the Laporte selection rule in an acentric oxygen environment.

Absorption spectra of the Cr^{3+} ion in monoclinic phase of the host system studied at 5 K are shown in Fig. 7. Table X contains the values of the energy levels with assignment for both phases. Separately, in Fig. 7 and Table XI the spectrum in the 13,700–14,000 cm^{-1} region is shown. The observed peaks indicate the presence of at least four (α–γ) Cr^{3+} sites. (See also Fig. 8.)

Emission Spectra

A broad band corresponding to the $^4T_2 \rightarrow {}^4A_2$ luminescence of aluminum tungstates was measured at room temperature by Pe-

TABLE V

FACTOR GROUP ANALYSIS FOR $Al_2(WO_4)_3$ CRYSTAL IN ORTHORHOMBIC PHASE ($Pbcn = D_{2h}^{14}$, $Z = 4$)

									Unit-cell modes					Activity	
D_{2h}	E	$C_2(z)$	$C_2(y)$	$C_2(x)$	i	$\sigma(xy)$	$\sigma(xz)$	$\sigma(yz)$	n(N)	n(T)	n(T′)	n(L)	$n(i)$	IR	Raman
A_g	1	1	1	1	1	1	1	1	25	0	7	4	14	—	xx,yy,zz
B_{1g}	1	1	−1	−1	1	1	−1	−1	26	0	8	5	13	—	xy
B_{2g}	1	−1	1	−1	1	−1	1	−1	25	0	7	4	14	—	xz
B_{3g}	1	−1	−1	1	1	−1	−1	1	26	0	8	5	13	—	yz
A_u	1	1	1	1	−1	−1	−1	−1	25	0	7	4	14	—	—
B_{1u}	1	1	−1	−1	−1	−1	1	1	26	1	7	5	13	T_z	—
B_{2u}	1	−1	1	−1	−1	1	−1	1	25	1	6	4	14	T_y	—
B_{3u}	1	−1	−1	1	−1	1	1	−1	26	1	7	5	13	T_x	—
									204	3	57	36	108		
U_R(p)	68	0	4	0	0	0	0	0							
U_R(s)	20	0	4	0	0	0	0	0							
U_R(s − ν)	12	0	4	0	0	0	0	0							
$[\chi(R)]_N$	204	0	−4	0	0	0	0	0							
$[\chi(R)]_T$	3	−1	−1	−1	−3	1	1	1							
$[\chi(R)]_{T'}$	57	1	−3	1	3	−1	−1	−1							
$[\chi(R)]_L$	36	0	−4	0	0	0	0	0							

Note. U_R(p) is the number of atoms remaining invariant under operation R; U_R(s), the number of ions whose center of symmetry remains invariant under operation R; U_R(s − ν), the number of polyatomic ions among U_R(s) ions; n(N), the number of total freedom; n(T), the number of translational motions of a crystal as a whole (acoustical modes); n(T′), the number of translational lattice modes; n(L), the number of librational lattice modes; $n(i)$, the number of internal modes in the complex ion; $[\chi(R)]$, the respective characters of the irreducible representations.

TABLE VI

CORRELATION DIAGRAM FOR THE INTERNAL VIBRATIONS OF THE WO_4^{2-} ION IN THE C_2 AND C_1 SITES OF THE $AL_2(WO_4)_3$ CRYSTAL

Molecular symmetry T_d	Site group symmetry	Factor group symmetry D_{2h}	Proposed assignment RS	Proposed assignment IR
		$C_2(\|b)$ symmetry		
		A_g	1050	
		A_u	—	—
A_1 $\nu_1 = 928$	A	B_{2g}	1049	
		B_{2u}		1041
		A_g	1025	
		A_u	—	—
	A	B_{2g}	1027	
		B_{2u}		1031
		B_{1g}	960	
F_2 $\nu_3 = 833$		B_{1u}	—	947
	B	B_{3g}	960	
		B_{3u}	—	
		B_{1g}	922	
		B_{1u}		922
	B	B_{3g}	921	
		B_{3u}		
		A_g	422	
		A_u	—	—
	A	B_{2g}	432	
		B_{2u}		420
		B_{1g}	428	
F_2 $\nu_4 = 405$		B_{1u}		440
	B	B_{3g}	425	
		B_{3u}		
		B_{1g}	387	
		B_{1u}		380
	B	B_{3g}	387	
		B_{3u}		
		A_g	330	
		A_u	—	—
	A	B_{2g}	334	
E $\nu_2 = 320$		B_{2u}		345
		A_g	300	
		A_u	—	—
	A	B_{2g}	300	
		B_{2u}		274
		C_1 symmetry		
		1	(1) 995	
		2		(2) —
		3	(3) 995	
A_1 $\nu = 928$	A	4		(4) 990
		5	(5) 997	
		6		(6) 1003
		7	(7) 997	
		8		(8)

TABLE VI—*Continued*

Molecular symmetry T_d	Site group symmetry	Factor group symmetry D_{2h}	Proposed assignment RS	Proposed assignment IR
		1	(1) 921	
		2		(2) —
		3	(3) 922	
		4		(4) 922
	A	5	(5) 921	
		6		(6) 945
		7	(7) 921	
		8		(8)
		1	(1) 897	
		2		(2) —
		3	(3)	
F_2 $\nu = 833$	A	4		(4) 892
		5	(5) 902	
		6		(6) 900
		7	(7) 900	
		8		(8)
		1	(1) 839	
		2		(2)
		3	(3) 840	
	A	4		(4) 866
		5	(5) 843	
		6		(6) 840
		7	(7) 837	
		8		(8)
		1	(1) 422	
		2		(2)
		3	(3) 428	
	A	4		(4) 440
		5	(5) 432	
		6		(6) 420
		7	(7) 425	
		8		(8)
		1	(1) 387	
		2		(2)
		3	(3) 387	
F_2 $\nu_4 = 405$	A	4		(4) 380
		5	(5) 393	
		6		(6)
		7	(7) 387	
		8		(8)
		1	(1) 377	
		2		(2)
		3	(3) 375	
	A	4		(4)
		5	(5) 375	
		6		(6) 378
		7	(7) 375	
		8		(8)

TABLE VI—*Continued*

Molecular symmetry T_d	Site group symmetry	Factor group symmetry D_{2h}	Proposed assignment RS	Proposed assignment IR
		1	(1) 330	
		2		(2) —
		3	(3) 335	
		4		(4) 337
	A	5	(5) 334	
		6		(6) 345
		7	(7) 332	
E	$\nu_2 = 320$	8		(8)
		1	(1)	
		2		(2) —
		3	(3) 289	
		4		(4) 294
	A	5	(5)	
		6		(6) 274
		7	(7) 282	
		8		(8)

Note. 1, A_g; 2, A_u; 3, B_{1g}; 4, B_{1u}; 5, B_{2g}; 6, B_{2u}; 7, B_{3g}; 8, B_{3u}.

termann and co-workers (*2, 4*). Crystals of $Al_{2-x}Cr_x(WO_4)_3$ manifest luminescence representative of Cr(III) systems in the intermediate crystal field $Dq/B = 2.31$. Such systems show narrow-band phosphorescence $^2E \rightarrow {}^4A_2$ and broad-band fluorescence $^4T_2 \rightarrow {}^4A_2$. The emission measurements were carried out in the temperature range 10–300 K (Fig. 9). The emission spectra at 10 K consist of a weak broad-band fluorescence $^4T_2 \rightarrow {}^4A_2$ with maximum centered at 785 nm and a group of intensive sharp lines $^2E \rightarrow {}^4A_2$ of phosphorescent origin, partially overlapped by the broad-band fluorescence. These well distinguished peaks may be assigned to the zero-phonon transitions and their vibronic sidebands. Some of the peaks depending on Cr concentration were assigned to the Cr–Cr pair transitions. The assignment proposed is given in Table XII.

With increasing temperature the intensities of phosphorescent lines decrease in relation to the broad-band fluorescence. With increasing temperature the peak of fluorescence shifts toward blue (see Fig. 9). This means that the minima of the ^2E and $^4T_2$ potential curves are clearly separated. In fact, the energy difference ΔE between the minima of the $^4T_2$ and the ^2E level is about 310 cm^{-1}, as could be expected for intermediate crystal field. The temperature dependence of emission lifetimes is shown for concentration $x = 0.004$ in Fig. 10a. The decay time of phosphorescence and the emission of Cr–Cr lines strongly depend on temperature in the range 11–70 K (e.g., drop from 600 to 187 μs for the phosphorescence). The lifetime decreases monotonically (see Fig. 10a). The fluorescence lifetime recorded at 12,853 cm^{-1} does not exhibit such dependence. In the range 11–60 K fluorescence decay time decreases from 112 to 62 μs. In the range 60–300 K the lifetime practically does not depend on temperature and changes from 60 to about 40 μs. The fluorescence lifetime depends on the concentration of Cr(III) ions. This dependence for phophorescence and fluorescence lifetimes measured at room temperature is shown in Fig. 10b. One can note that both curves describing the concentration effect are similar.

Fig. 11 shows "phosphorescent" transi-

TABLE VII

A_g, B_{1g}, B_{2g}, B_{3g} AND B_{1u}, B_{2u} FUNDAMENTAL FREQUENCIES FOR ORTHORHOMBIC $Al_2(WO_4)_3$ SINGLE CRYSTAL

Raman spectra				IR spectra	
A_g	B_{1g}	B_{2g}	B_{3g}	B_{1u}	B_{2u}
				$2029 = 1050A_g + 990B_{1u}$	$2030 = 995A_g + 1035B_{3u}$[a]
				$1936 = 1050A_g + 892B_{1u}$	$1924 = 1025A_g + 899B_{3u}$ or $921A_g + 1003B_{3u}$
				$1911 = 921A_g + 990B_{1u}$	—
				$1874 = 960A_g + 922B_{1u}$	$1872 = 1025A_g + 847B_{3u}$ or $839A_g + 1035B_{3u}$
				$1735 = 839A_g + 892B_{1u}$	$1742 = 839A_g + 899B_{3u}$
				—	$1700 = 839A_g + 861B_{3u}$
				—	$1536 = 1050A_g + 486B_{3u}$
				$1468 = 422A_g + 1049B_{1u}$	$1471 = 1050A_g + 421B_{3u}$ or $422A_g + 1049G_{eu}$
				$1447 = 422A_g + 1024B_{1u}$	$1446 = 1025A_g + 421B_{eu}$
				$1320 = 1050A_g + 271B_{1u}$	$1320 = 1050A_g + 270B_{3u}$ or $422A_g + 899B_{3u}$
				$1278 = 387A_g + 892B_{1u}$	$1279 = 839A_g + 440B_{3u}$ or $387A + 899B_{3u}$
				—	$1126 = 921A_g + 205B_{3u}$ or $300A_g + 826B_{3u}$
1050vs	1050s	1049vs	1049vs	1049s	1041m
1025m	1025s	1027sh	1026m	1024m	1031m
995w	995w	997w	997w	990m	1003sh
960w	960w	960w	960w	—	967s
—	—	—	—	947sh	945sh
921m	922s	922w	921m	922s	—
897w	—	902w	900w	892s	900s
839w	840vw	843w	837w	866s	840s
—	—	—	—	—	602sh
—	—	—	—	—	574sh
—	—	—	—	—	532m
—	—	—	—	515m	500m
422w	428w	432w	425w	440m	420m
387m	387vs	393w	387s	—	—
377m	375sh	375sh	375sh	380w	378w
330w	335w	334w	332sh	337m	345m
300w	—	300vw	296w	294m	—
—	289w	—	282w	271m	274m
259w	245w	240vw	246w	241w	244m
—	—	—	222w	219w	219m
202w	200vw	—	199w	206w	207m
—	—	—	—	192m	195w
165w	163w	176w	165w	—	172w
—	150w	—	159w	159w	161w
—	—	—	—	145w	—
—	—	—	—	136w	—
124w	124w	123w	124w	127w	123w
—	—	—	—	116w	—
102w	102w	103w	—	98w	105w
—	87w	89w	90w	—	94w
—	—	—	—	70w	—

* B_{3u} modes were evaluated from two-phonon transitions.

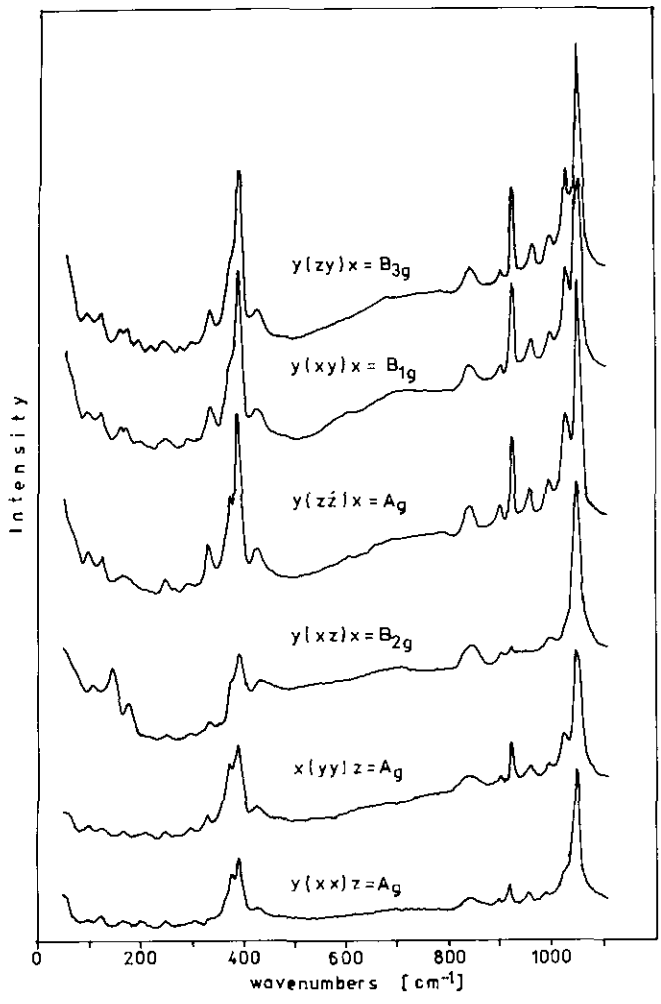

FIG. 3. Polarized Raman spectra of the $Al_2(WO_4)_3$ single crystal at 293 K.

TABLE VIII

FACTOR GROUP ANALYSIS FOR $Al_2(WO_4)_3$ CRYSTAL IN MONOCLINIC PHASE ($P2_1 = C_2^2$, $Z = 4$)

C_2	E	$2_1(y)$	n(N)	n(T)	n(T′)	n(L)	$n(i)$	IR	RS
A	1	1	102	1	29	18	54	y	x^2,y^2,z^2,xy
B	1	−1	102	2	28	18	54	x,y	xy,yz
			204	3	57	36	108		
U_R(p)	68	0							
U_R(s)	20	0							
U_R(s − ν)	12	0							
$[\chi(R)]_N$	204	0							
$[\chi(R)]_T$	3	−1							
$[\chi(R)]_{T'}$	57	1							
$[\chi(r)]_L$	36	0							

Note. The meaning of U_R, χ, and n is specified in the Note to Table V.

TABLE IX

IR AND RS FREQUENCIES OF POLYCRYSTALLINE $Al_2(WO_4)_3$ IN ORTHORHOMBIC (300 K) AND MONOCLINIC PHASES (14 K)

IR spectra		RS spectrum	
300 K	14 K	300 K	Assignment
	1081		
1075sh			
	1075		
	1055		
1033m	1040		
	1032	1047s	
	1024		
1013			
	1016		
975sh	976	992w	W–O stretching vibrations
	921	961w	
909vs			
	902	923m	
	889		
892vs			
	870	898w	
	847		
832vs	826		
	813	844w	
771	—		
612w	610		
576vw	575		
	468		
447s	450		
	431	426w	
	404		
389s	392		
	380	392vs	
	373		
354s	367		Bending δ(OWO)
	355	377sh	vibrations
	340		
336sh			
	321	340w	
	315		
310m			
	307		
300m	298	300w	
281	285		
	276		
271			
	271		Essentially T′(Al^{3+})
234	235w	250w	Essentially T′(WO_6)
203	211		
190w	199		
163w	169	168w	
		126w	
		102w	
125w	119	60w	Essentially L(WO_6)

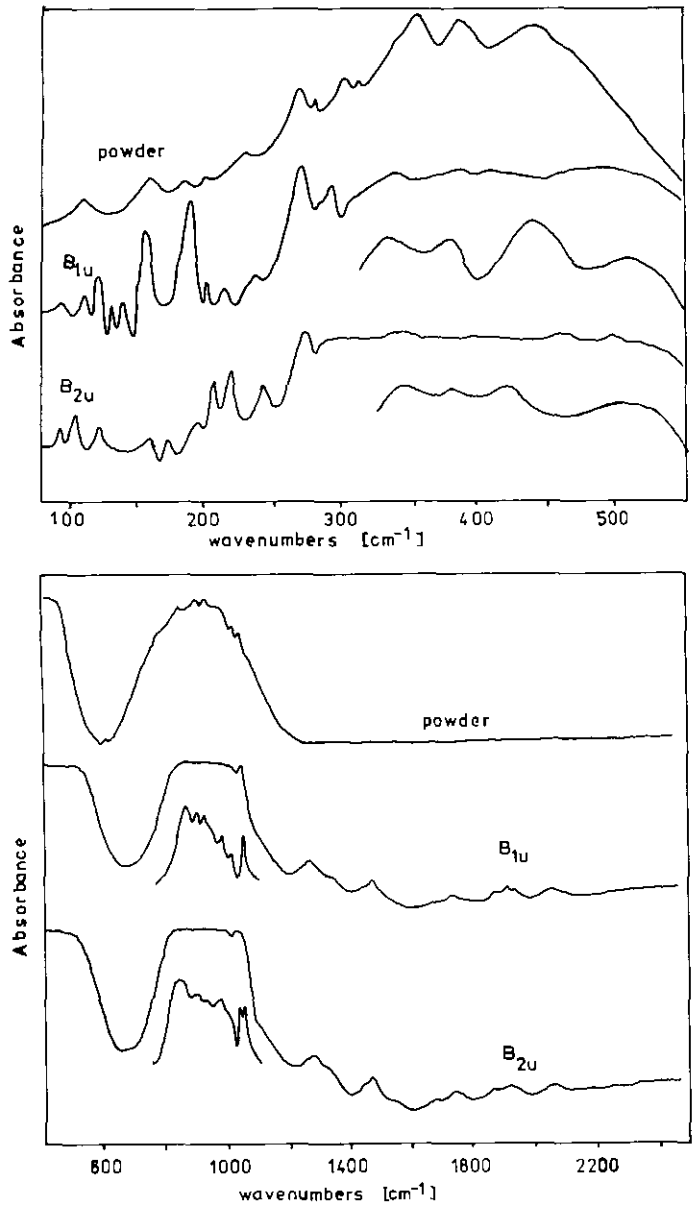

FIG. 4. IR spectra of the powder sample and $Al_2(WO_4)_3$ single crystal at 293 K.

tions in an expanded scale measured at 10 K. The positions of successive lines were assigned to the zero-phonon and phonon sidebands of the different Cr(III) sites. The number of lines corresponding to Cr(III) sites does not depend on the excitation wavelength. Following the above assignment we identify four most pronounced Cr(III) sites giving contribution to the spectra. The character of the broad band fluorescence suggests strong electron–phonon coupling. All these phonons are connected with the oxygen, involving vibrations of the first coordination sphere of active ions.

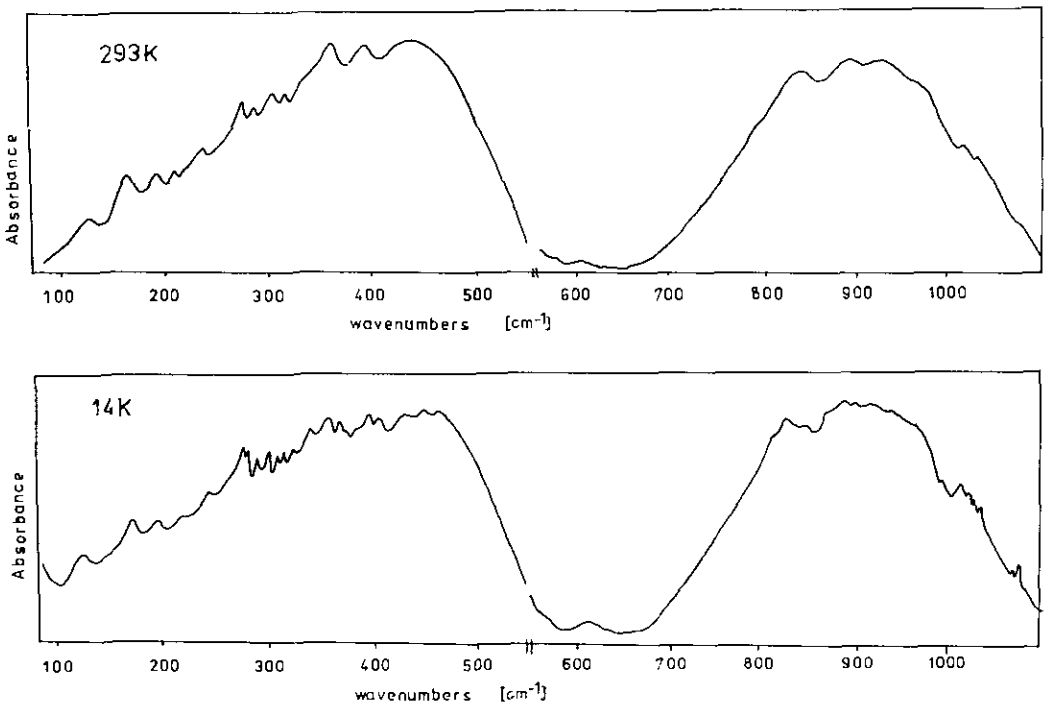

FIG. 5. Comparison of the IR of polycrystalline $AL_2(WO_4)_3$ at 292 and 14 K.

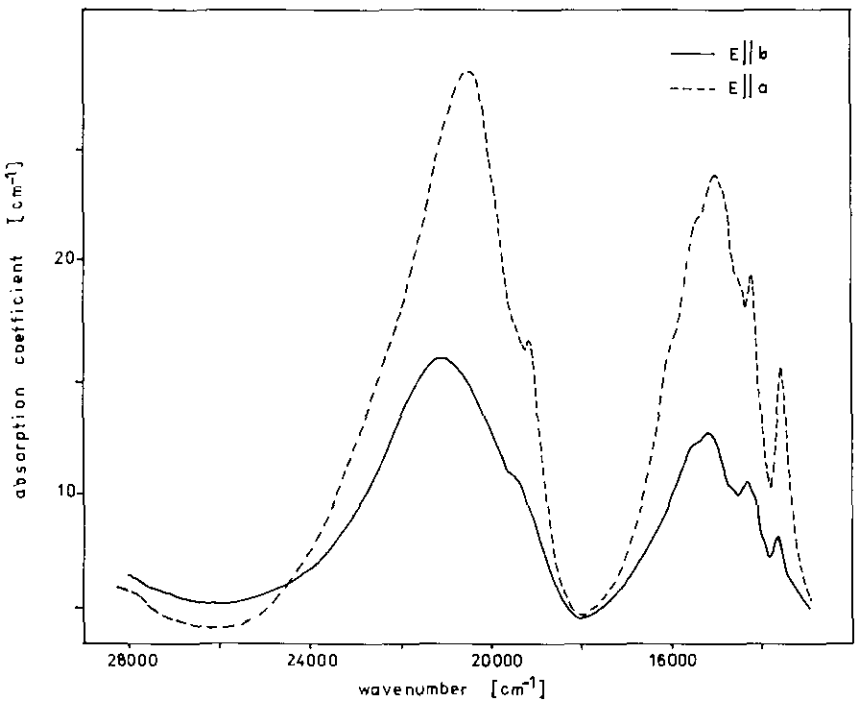

FIG. 6. The polarized absorption spectra of $Al_{1.96}Cr_{0.04}(WO_4)_3$ crystal. The absolute peak intensity is about 4×10^{-19} cm^2 for E$\|$b and $x = 0.02$.

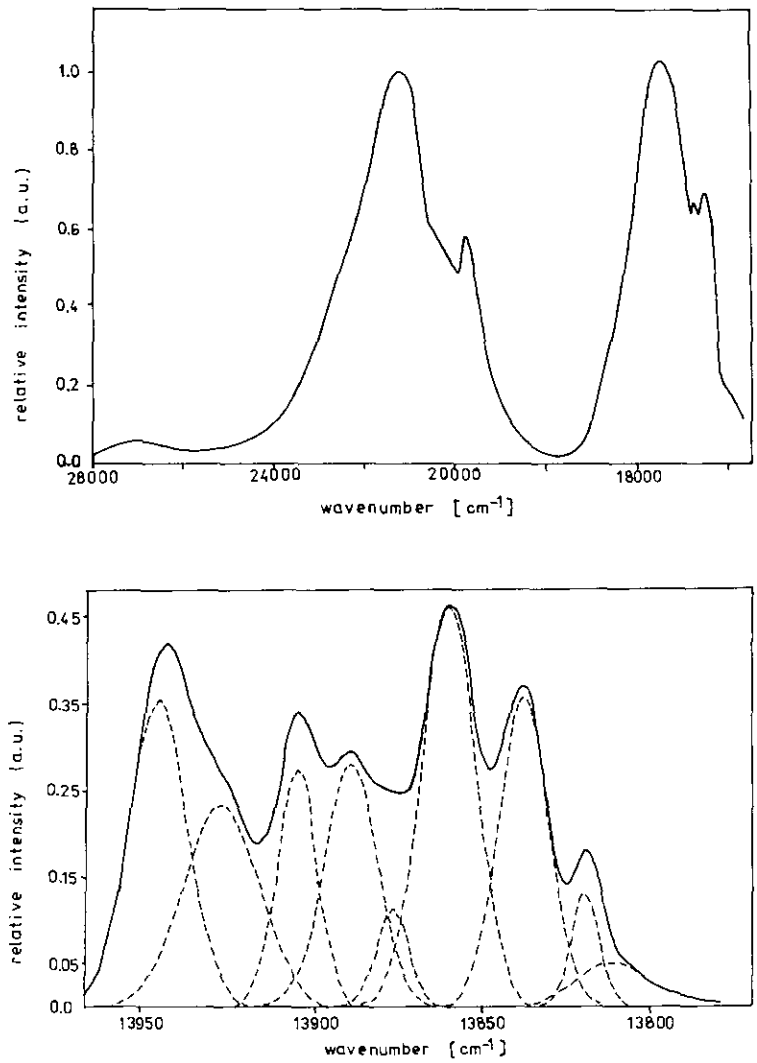

FIG. 7. Electron absorption spectra of the monoclinic phase of the $Al_{2-x}Cr_x(WO_4)_3$ crystal and their Gaussian deconvolution.

These phonons should be considered as promoting modes of $^4T_{2g} \rightarrow {}^4A_{2g}$ fluorescence.

Conclusions

$Al_{2-x}Cr_x(WO_4)_3$ crystals are promising luminescent materials. They exhibit a broad band $^4T_2 \rightarrow {}^4A_2$ fluorescence, characteristic of low field ligand strength, and simultaneously they show $^2E \rightarrow {}^4A_2$ phosphorescence, characteristic of strong ligand fields. The Dq/B parameter equal to 2.31 suggests an intermediate ligand field. The nearest environment of the activator changes from pseudotetragonal in rhombic phase to triclinic in low-temperature phase. One active site and four Cr^{3+} site centers can be distinguished

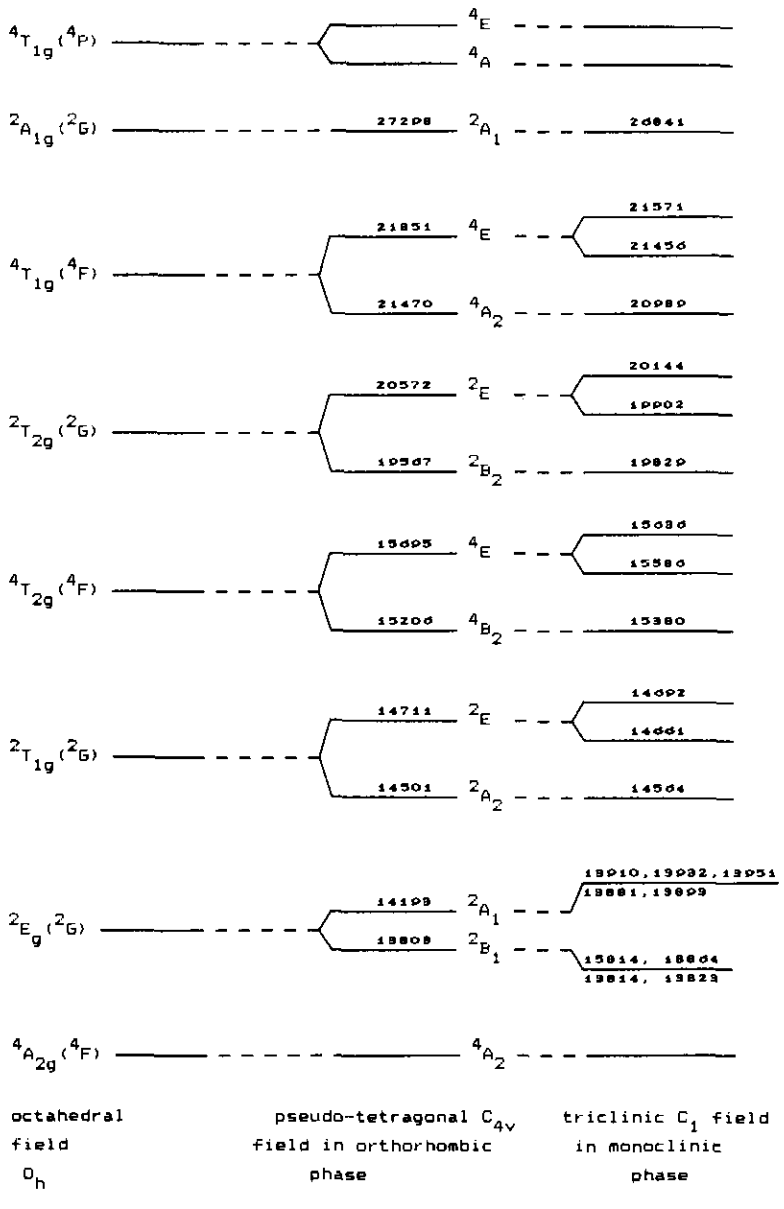

FIG. 8. Crystal field splitting of the Cr^{3+} levels for orthorhombic and monoclinic phases of $AL_2(WO_4)_3$ (energies in cm^{-1}).

TABLE X

EXPERIMENTAL ENERGIES FOR ORTHORHOMBIC AND MONOCLINIC PHASES OF $Al_{1.98}Cr_{0.02}(WO_4)_3$ FROM ABSORPTION SPECTRUM MEASURED AT 293 AND 5 K, RESPECTIVELY

Energy (experimental data) cm^{-1}		
Orthorhombic phase	Monoclinic phase	Assignment in O_h group notation
27,777	27,027	$^4T_1(P)$
22,222	22,727	
21,413	21,552	$^4T_1$
20,833	21,186	
	20,161	
19,685	19,881	$^2T_2$
	19,763	
16,234	16,447	
15,625	15,551	$^4T_2$
15,267	15,314	
14,815	14,859	
14,535	14,728	$^2T_1$
	14,663	
	14,577	
13,812	13,951	
	13,935	
	13,908	
	13,893	
	13,885	^2E
	13,866	
	13,843	
	13,824	
	13,812	

TABLE XII

EMISSION LINES OF Cr^{3+} IN $Al_2(WO_4)_3$ AT 10 K

Frequency $[cm^{-1}]$		Assignment
13,948		zero-phonon line δ $^2E_g \rightarrow {}^4A_{2g}$
13,908	$2\overline{A}$	zero-phonon lines γ
13,905	$\overline{E}$	$^2E_g \rightarrow {}^4A_{2g}$
13,850	$2\overline{A}$	zero-phonon lines β
13,846	$\overline{E}$	$^2E_g \rightarrow {}^4A_{2g}$
13,824	$2\overline{A}$	zero-phonon lines α
13,820	$\overline{E}$	$^2E_g \rightarrow {}^4A_{2g}$
13,759		
13,755		poorly resolved
13,750		zero-phonon lines
13,744		of other sites
13,736		
13,733		
13,465		
13,441		
13,426		pair lines
13,399		
13,366		
13,320		
12,850		$^4T_{2g} \rightarrow {}^4A_{2g}$

TABLE XI

EXPERIMENTAL AND EVALUATED ENERGIES WITH GAUSSIAN DECONVOLUTION DATE FOR MONOCLINIC PHASE OF $Al_{1.98}Cr_{0.02}(WO_4)_3$ FOR $^4A_2 \rightarrow {}^2E$ TRANSITIONS

Experimental data $[cm^{-1}]$	Gaussian deconvolution			Type of center of Cr^{+3}
	Energy	Width	Maximum intensity	
13,951	13,951	20.8	0.355	
13,935	13,932	26.4	0.236	δ
13,908	13,910	13.9	0.276	
13,893	13,893	18.4	0.284	
13,885	13,881	11.0	0.115	γ
13,866	13,864	18.9	0.461	
13,843	13,842	17.0	0.359	β
13,824	13,823	9.4	0.132	
13,812	13,814	24.3	0.052	α

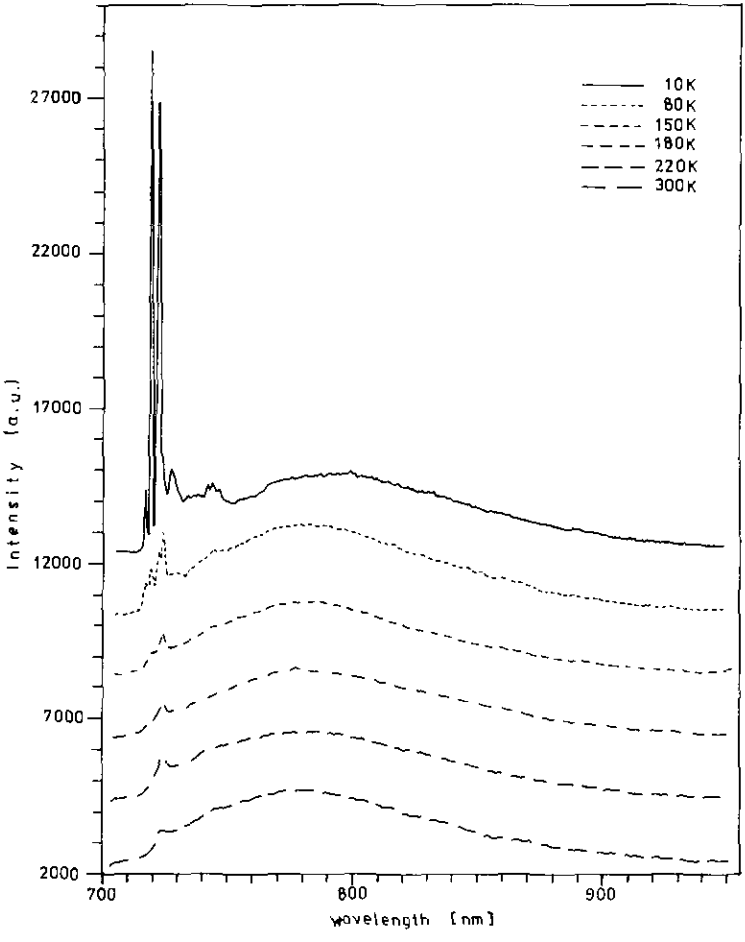

FIG. 9. Luminescence spectra of the $Al_{1.99}Cr_{0.01}(WO_4)_3$ single crystal.

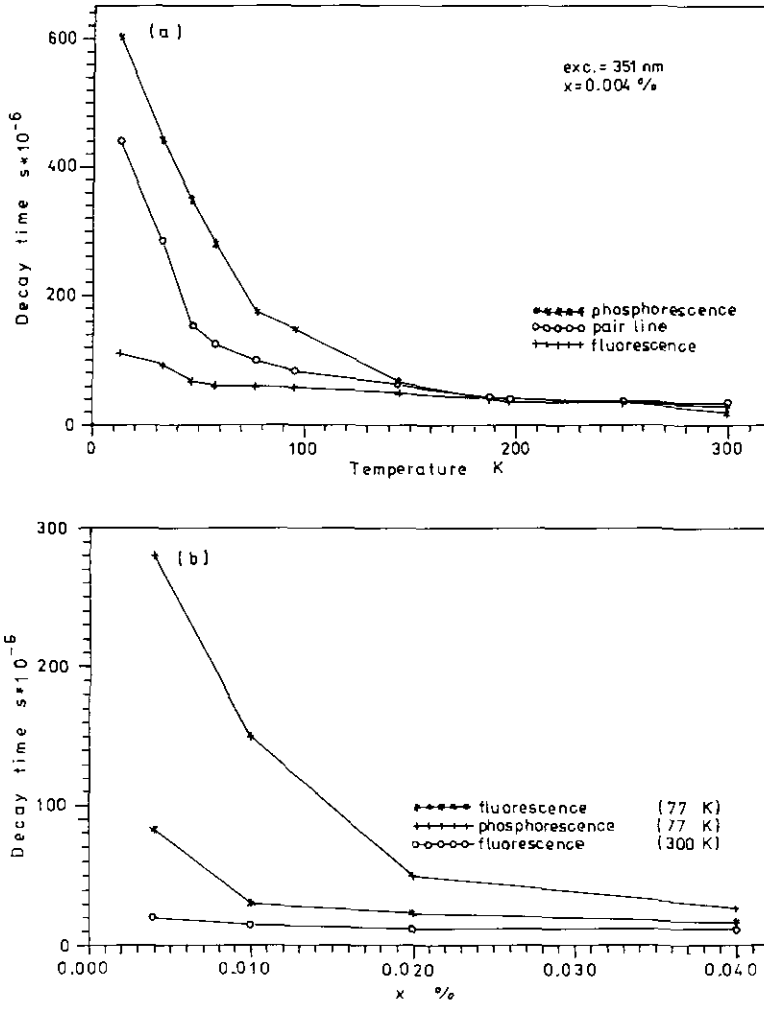

FIG. 10. Fluorescence decay curves of $Al_{2-x}Cr_x(WO_4)_3$: (a) the temperature dependence of emission lifetimes for concentration $x = 0.004$; (b) the concentration dependence of phosphorescence and fluorescence lifetimes at RT and 77 K.

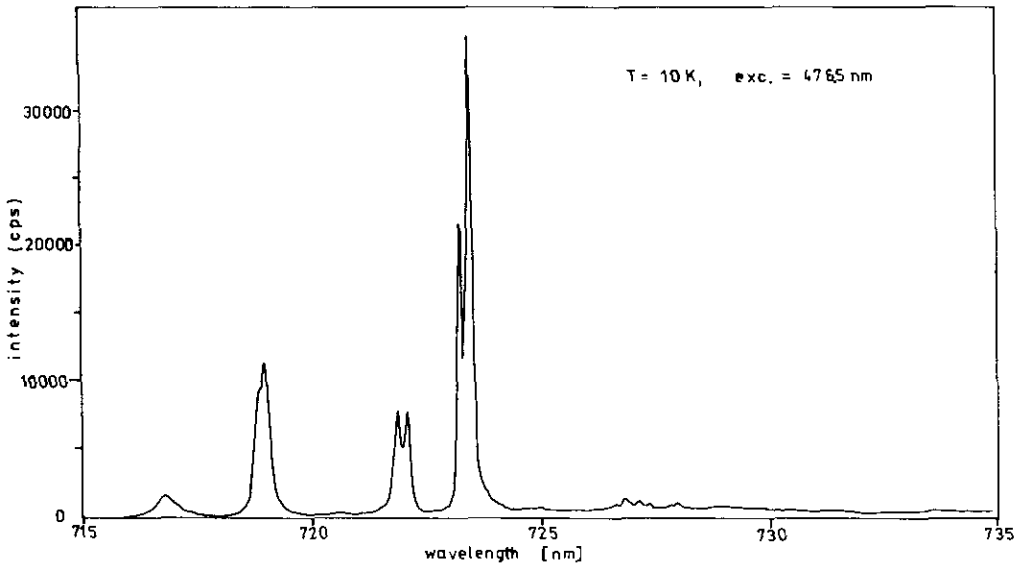

FIG. 11. The $^2E \rightarrow {}^4A_2$ emission of the $Al_{2-x}Cr_x(WO_4)_3$ crystal at 10 K in expanded scale.

in the orthorhombic and monoclinic phase, respectively. The dynamics and mechanism of the energy transfer process in the material studied will be analyzed in detail elsewhere.

Acknowledgments

We gratefully acknowledge the constructive criticisms of the referees. This work was supported by the Polish State Committee for Scientific Research, Grant 2 0832 91 01.

References

1. A. E. NOSENKO AND D. L. L. FUTORSKI, *Opt. Spektrosk.* **34,** 286 (1973).
2. K. PETERMAN AND G. HUBER, *J. Lumin.* **31–32,** 71 (1984).
3. W. KOLBE, K. PETERMANN, AND G. HUBER, *IEEE J. Quantum Electron.* **QE-21,** 1596 (1985).
4. K. PETERMANN AND P. MITZSCHERLICH, *IEEE J. Quantum Electron.* **QE-23,** 1122 (1987).
5. W. J. WORONKOVA, W. K. JANOWSKIJ, AND W. A. KOPCIK, *Vestn. Mosk. Univ. Ser. 3* **3,** 109 (1968).
6. J. J. DE BOER, *Acta Crystallogr. Sect. B* **30,** 1878 (1974).
7. D. C. CRAIG AND N. C. STEPHENSON, *Acta Crystallogr. Sect. B* **27,** 1250 (1968).
8. H. SIEBERT, *Z. Anorg. Allg. Chem.* **273,** 21 (1954).
9. L. A. WOODWARD AND H. L. ROBERTS, *Trans. Faraday Soc.* **52,** 615 (1956).
10. M. L. BANSAL, *in* "Raman Spectroscopy; Sixty Years On" (H. D. Bist, I. R. During, and I. F. Sullivan, Eds.), Vibrational Spectra and Structure, Vol. 17A, pp. 11–25, Elsevier, Amsterdam, 1989.